Insertion of Triangulated Surfaces Into a Meccano Tetrahedral Discretization by Means of Mesh Refinement and Optimization Procedures

Eloi Ruiz-Gironés[a], Albert Oliver[b], Guillermo V. Socorro-Marrero[b], José M. Cascón[c], Eduardo Rodríguez[b], José M. Escobar[b], Rafael Montenegro[b], José Sarrate[a]

[a] *Laboratori de Càlcul Numèric (LaCàN), www.lacan.upc.edu*
Departament d'Enginyeria Civil i Ambiental, ETSECCPB,
Universitat Politècnica de Catalunya - BarcelonaTech
Jordi Girona 1-3, 08034 Barcelona, Spain
[b] *University Institute for Intelligent Systems and Numerical Applications in Engineering (SIANI), www.dca.iusiani.ulpgc.es/proyecto2015-2017*
University of Las Palmas de Gran Canaria,
Campus de Tafira, 35017 Las Palmas, Spain
[c] *Grupo de Investigación en Simulación Numérica y Cálculo Científico, diarium.usal.es/sinumcc/*
Department of Economics and Economic History,
Faculty of Economics and Business,
University of Salamanca,
37007 Salamanca, Spain

Abstract

In this paper, we present a new method for inserting several triangulated surfaces into an existing tetrahedral mesh generated by the meccano method. The result is a conformal mesh where each inserted surface is approximated by a set of faces of the resulting tetrahedral mesh. First, the tetrahedral mesh is refined around the inserted surfaces to capture their geometric features. Second, each immersed surface is approximated by a set of faces from the tetrahedral mesh. Third, following a novel approach the nodes of the approximated surfaces are mapped to the corresponding immersed surface. Fourth, we untangle and smooth the mesh by optimizing a regularized shape distortion measure for tetrahedral elements in which we move all the nodes of the mesh, restricting the movement of the edge and surface nodes along the corresponding entity they belong to. The refining process allows approximating the immersed surface for

Email addresses: eloi.ruiz@upc.edu (Eloi Ruiz-Gironés), albert.oliver@ulpgc.es (Albert Oliver), gvsocorro@siani.es (Guillermo V. Socorro-Marrero), casbar@usal.es (José M. Cascón), eduardo.rodriguez@ulpgc.es (Eduardo Rodríguez), josem.escobar@ulgpc.es (José M. Escobar), rafael.montenegro@ulpgc.es (Rafael Montenegro), jose.sarrate@upc.edu (José Sarrate)

any initial tetrahedral mesh. Moreover, the proposed projection method avoids computational expensive geometric projections. Finally the applied untangling and smoothing process delivers a high-quality mesh and ensures that the immersed surfaces are interpolated.

Keywords: Surface Insertion, Meccano Method,
Tetrahedral Mesh Generation, Mesh Untangling and Smoothing,
Surface Parameterization, Volume Parameterization

---

1. Introduction

In most of the computational simulations in applied sciences and engineering, the geometry, delimited by outer surfaces and probably including inner surfaces, is usually a given data. However, in a wide range of applications, it is not possible to generate *a priori* a mesh that contains the inner surfaces, since it may be an unknown of the problem. This is the case of immiscible multi-fluid problems in which the interface between fluids evolves in time, and its location depends on the physics of the problem. Another situation is that the exact location of the surface may be known in advance nevertheless it changes over time. In this case, a new mesh for each time step has to be generated. For instance, in computational fluid dynamics, the motion of a rotating propeller is prescribed, and the surface position is known at each time step. Moreover, during an advanced stage of a design process, a new geometric feature can be added to an already discretized model. The additional surfaces impose the generation of a new discretized model that reproduces the new surface. For example, a new fault has to be inserted in an already meshed oil reservoir.

Several numerical strategies can be adopted to deal with this problem. It is possible to design sophisticated solvers to track the new or moving surfaces. For example, the phase-field approach consists of adding new unknown fields in the governing equations. The surfaces are defined as the zero level set of the additional field unknowns [1, 2, 3]. The extended finite element method (X-FEM) formulation [4, 5, 6] adds new shape functions to include discontinuities in the solution. Thus, the surface to be added is defined using these discontinuities.

Nevertheless, it is not always possible to modify the solver to include these techniques. Therefore, it is necessary to modify the mesh in order to approx-

imate the additional or moving surfaces using the triangles of the tetrahedral mesh. A straightforward solution is to generate an entirely new mesh for the geometric model. However, this is a costly operation, especially if it has to be performed in all the time steps of a transient problem. Thus, other approaches have been developed to reduce the computational cost of generating a new mesh. On the one hand, it is possible to approximate the surface by performing a mesh moving technique, see [7, 8, 9]. First, it is selected a set of triangles to approximate the surface. Then, these triangles are moved onto the surface while keeping valid elements. To perform this process, the size of the tetrahedral mesh has to be small enough to reproduce the geometric features of the immersed surface. On the other hand, the tetrahedral mesh can be locally remeshed in order to approximate the given surface, see [10, 11, 12]. First, a triangular mesh on the surface is generated, and the tetrahedral elements that are *near* the surface are removed. Then, the created cavity is remeshed to generate a conformal mesh that includes the surface. Note that the cavity has to be large enough to accommodate the new elements, and small enough to keep the number of modified elements as small as possible.

In this work we propose a novel approach to insert a given triangulated surface into an existing tetrahedral mesh generated using the meccano method [13, 14, 15, 16]. It combines the benefits of local remeshing processes and mesh moving techniques. First, we locally refine the tetrahedral mesh around the surface until the tetrahedral mesh captures the geometric features of the surface. Specifically, we use the Kossaczký method that delivers a fast and robust process, since it does not depend on geometric predicates. Second, we select a set of triangles of the tetrahedral mesh to approximate the surface. To this end, we use a set of rules to ensure that a high-quality mesh can be obtained. Second, we propose a new projection algorithm based on the Floater parameterization [17] of the immersed and approximating surfaces. We highlight that we use the same parametric space for both surfaces. Therefore, we can define a mapping from the approximating surface onto the immersed one. We use this mapping to ensure that the projected nodes lie on the immersed surface. The projection step introduces inverted and low-quality elements. Thus, in the fourth step, we optimize the quality of the final mesh by using a robust untangling and

smoothing process based on an optimization of a single distortion measure [18]. Specifically, we optimize a regularized version of the shape distortion measure for tetrahedral elements in which we move all the nodes of the mesh, restricting the movement of the edge and surface nodes along the corresponding entity they belong to [19]. This is achieved by expressing the coordinates of these nodes in terms of their parametric coordinates during the optimization process. Although the target of the optimization process is the distortion of the tetrahedra, the method also improves the quality of the triangles that approximate the surfaces of the model since we allow moving the surface nodes.

The proposed method has several advantages. It is independent of the initial mesh because of the refinement process that adapts the mesh to the features of the immersed surface. Moreover, we propose a fast and robust projection process that involves solving two linear problems. One for all the nodes of the immersed surface, and another one for all the nodes of the approximating surface. In this way, we avoid solving the non-linear problem involved in the geometric projection to the immersed surface of each node of the approximating surface. Finally, the applied untangling and smoothing process ensures a valid and high-quality mesh that interpolates the immersed surface.

The rest of the paper is structured as follows. In Section 2 we overview the meccano method. In Section 3 we detail the proposed algorithm to insert a given surface in a tetrahedral meccano mesh. Finally, in Section 4, we present three examples, both academic and realistic, illustrating the capabilities of the proposed method.

2. Meccano overview

The meccano method [13, 14, 15, 16] is an automatic tetrahedral mesh generator for complex genus-zero solids. The method requires a surface triangulation of the solid boundaries and a computational domain that coarsely approximates the solid. This computational domain is called meccano. The procedure builds an adaptive tetrahedral mesh in the meccano and deforms it to match the physical domain. For this purpose, the method combines several procedures: an automatic mapping from the boundary of the meccano to the boundary of the solid, a 3-D local refinement algorithm, and a simultaneous mesh untangling and

smoothing. It is important to point out that this method also provides a continuous element-wise linear volumetric parameterization from the computational domain to the genus-zero solid.

The main steps of the meccano tetrahedral mesh generation algorithm are summarized in Algorithm 1. The input data is a solid, Ω, defined by its boundary representation (surface triangulation or CAD model), and a given precision to approximate its boundary, ε.

The first step of the procedure, Line 2, is to construct a meccano, $\mathcal{D}$, that approximates the solid, by connecting polyhedral pieces. Although the construction of the meccano is not automatic in general, in certain cases it can be performed with no manual interaction, see [15]. Then, in Line 3, a discrete mapping, $\mathbf{\Pi}$, between the boundary of the meccano and the boundary of the solid is computed using the mean value parametrization proposed in [17]. Note that the parameterization obtained from the Floater method is a continuous and element-wise linear mapping. In Line 4, an initial coarse mesh of the meccano is generated, and the boundary nodes are located on the solid boundary using the mapping $\mathbf{\Pi}$. In Lines 5–9, we obtain a mesh that approximates the solid boundary with the given tolerance ε. Specifically, in Line 6, we get the list of triangles that do not correctly approximate the boundary of the solid, and then, in Line 7, we refine those triangles by dividing their adjacent tetrahedra using the Kossaczký method [20]. In Line 8, we project the new nodes onto the boundary of the solid using the mapping $\mathbf{\Pi}$. We iterate this process until there are no triangles to refine. Note that when the nodes are mapped onto the solid boundary, low-quality and inverted elements may appear. Thus, a simultaneous untangling and smoothing procedure [18, 21] is applied in order to obtain a valid and high-quality tetrahedral mesh.

3. Surface insertion algorithm

In this section, we detail the proposed algorithm to insert a surface into an existing tetrahedral mesh generated using the meccano method. Although we describe the algorithm inserting a single surface, it can be extended to the insertion of several surfaces. To illustrate the process, we show a 2D analogy.

Algorithm 1 Meccano tetrahedral mesh generation.

```
1: function MeccanoMesher(Solid Ω, Real ε)
2:     Meccano 𝒟 ← getMeccano(Ω)
3:     Mapping Π ← getBoundaryMapping(𝒟, Ω)
4:     Mesh ℳ ← getInitialMesh(𝒟, Π)
5:     while distance(∂ℳ, ∂Ω) > ε do
6:         TriangleList τ ← getTrianglesToRefine(ℳ, Ω, ε)
7:         TriangleList τ' ←refineTriangles(τ)
8:         projectNewNodesToBoundary(τ', Π)
9:     end while
10:    qualityOptimization(ℳ)
11: end function
```

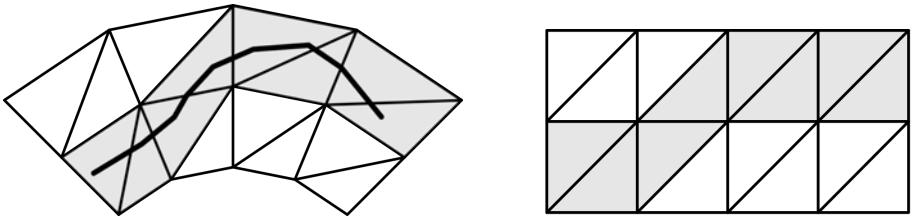

(a) (b)

Figure 1: Initial meccano mesh and immersed polyline S (thick line). (a) Physical mesh; (b) computational mesh.

3.1. Problem Statement

Our input data is a tetrahedral mesh $\mathcal{M}$ generated by the meccano method, composed of M tetrahedra, and an immersed triangular mesh $\mathcal{S}$, containing N triangles. We assume that $\mathcal{S}$ is simply connected, single oriented, and has a boundary. Figure 1 shows the initial meccano mesh for a two-dimensional geometry, and a polyline $\mathcal{S}$ to be inserted in the mesh.

Our target is to construct a surface $\mathcal{S}_{\mathcal{M}}$ composed of triangles, edges, and vertices belonging to a conformal tetrahedral mesh, obtained by refining $\mathcal{M}$, which approximates $\mathcal{S}$ with a given tolerance.

3.2. Volumetric Approximation

We define $\mathcal{T}$ as the set of tetrahedra of $\mathcal{M}$ that intersect the inserted surface, $\mathcal{S}$. Then, we recursively update the set $\mathcal{T}$ by refining those tetrahedra $E \in \mathcal{T}$

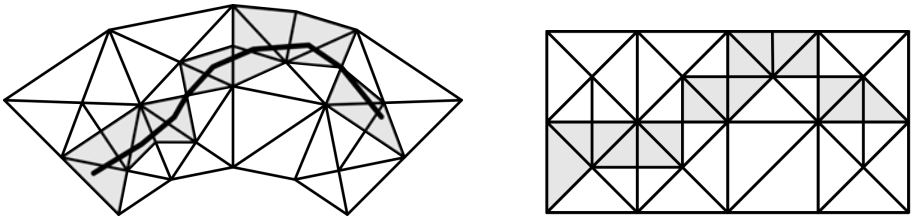

(a) (b)

Figure 2: Refined meccano mesh around the immersed polyline $\mathcal{S}$. (a) Physical mesh; (b) computational mesh.

such that

$$r_c^E \geq l_c, \qquad E \in \mathcal{T} \tag{1}$$

where r_c^E is the circumradius of the element E, and l_c is characteristic length of $\mathcal{S}$ provided by the user according to the geometric features of $\mathcal{S}$. To refine the tetrahedra, we apply the Kossaczký method. The original tetrahedra are removed from $\mathcal{T}$, and the refined ones that intersect $\mathcal{S}$ are added. This process is iterated until there is no tetrahedron in $\mathcal{T}$ that verifies condition (1). Figure 2 shows the refinement process of the mesh $\mathcal{M}$ and the triangles that intersect $\mathcal{S}$.

3.3. Volumetric Approximation Healing

In order to obtain a high-quality mesh, we need to impose the following constraints to the set of tetrahedra $\mathcal{T}$. First, we add elements to $\mathcal{T}$ until its boundary is topologically equivalent to the boundary of a sphere, Figure 3. To this end, we ensure that all the nodes that belong to the boundary of $\mathcal{T}$ define a local disk. That is, the Euler characteristic, χ, of each node on the boundary $\mathcal{T}$ verifies:

$$\chi := n_E - n_F + n_C = 1, \tag{2}$$

where n_E, n_F and n_C are the number of edges, faces, and cells of $\mathcal{T}$ that are adjacent to the node. Thus, we add the elements adjacent to the nodes that do not verify condition (2).

Then, we enforce that the counterpart of the boundary faces and edges in the computational space are parallel to the coordinate axis, Figure 4. This is accomplished by adding additional tetrahedra into the set $\mathcal{T}$. First, we identify the faces in the computational domain that are not parallel to the axis. Then,

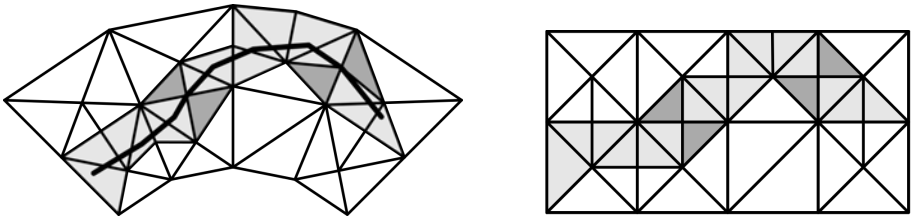

(a) (b)

Figure 3: Extension of $\mathcal{T}$ to be topologically equivalent to a sphere. (a) Physical mesh; (b) computational mesh.

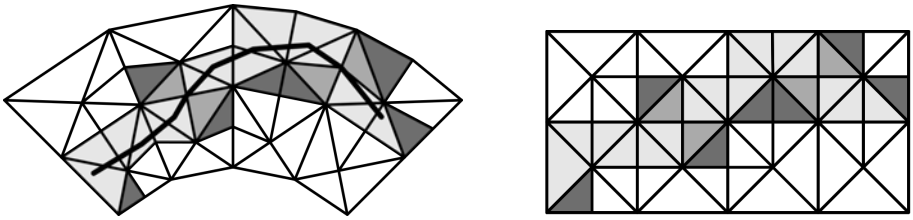

(a) (b)

Figure 4: Extension of $\mathcal{T}$ to get boundary edges parallel to the computational axis. (a) Physical mesh; (b) computational mesh.

we refine the adjacent tetrahedra to the same refinement level. Finally, we add the new tetrahedra into $\mathcal{T}$. This process ensures that we minimize the number of added tetrahedra into $\mathcal{T}$.

3.4. Surface Extraction

The set of tetrahedra $\mathcal{T}$ contains the given surface $\mathcal{S}$ completely in its interior. We will obtain $\mathcal{S}_{\mathcal{M}}$, the approximation of $\mathcal{S}$, from the boundary faces of $\mathcal{T}$. The main idea is to select the faces of the boundary of $\mathcal{T}$ that are at one *side* of the inserted surface, $\mathcal{S}$, and are not adjacent to any other surfaces of the model. We first classify the boundary nodes of $\mathcal{T}$ according to the side of $\mathcal{S}$ they are located. Figure 5a depicts the nodal classification of the boundary nodes of $\mathcal{T}$ using black and white circles. Then, we select the boundary triangles of $\mathcal{T}$ that have all the nodes classified in the same side of $\mathcal{S}$ and are not adjacent to any other surface of the model.

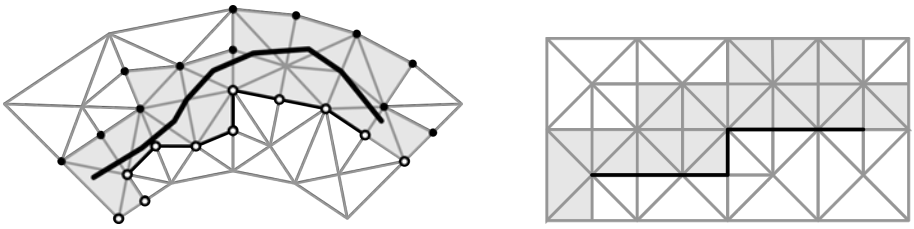

(a) (b)

Figure 5: Initial selection of $\mathcal{S}_\mathcal{M}$. (a) Physical mesh and classification of boundary nodes of $\mathcal{T}$ according the side of $\mathcal{S}$ they are located; (b) computational mesh.

3.5. Surface Healing

To increase the quality of the mesh and avoid inverted elements, we apply the following steps to $\mathcal{S}_\mathcal{M}$.

1. *Remove thin protrusions at the boundary of* $\mathcal{S}_\mathcal{M}$. We define thin protrusions as pairs of connected triangles of $\mathcal{S}_\mathcal{M}$ with three edges at the boundary of $\mathcal{S}_\mathcal{M}$. Thin protrusions at the boundary of $\mathcal{S}_\mathcal{M}$ may induce low-quality elements in the tetrahedral mesh. Thus, we recursively remove all thin protrusions in the surface approximation, see Figure 6a.

2. *Remove high-connectivity nodes at the boundary of* $\mathcal{S}_\mathcal{M}$. Nodes at the boundary of $\mathcal{S}_\mathcal{M}$ that are adjacent to five or more triangles in $\mathcal{S}_\mathcal{M}$ may induce low-quality elements in the final mesh. To solve this issue, we add the adjacent face to $\mathcal{S}_\mathcal{M}$, see Figure 6b. The two edges of the boundary of $\mathcal{S}_\mathcal{M}$ adjacent to the node, define a plane in the computational domain. We add the faces of the boundary of $\mathcal{T}$ that belong to this plane and are adjacent to the boundary edges.

3. *Refine tetrahedra with more than one face on* $\mathcal{S}_\mathcal{M}$. In order to avoid tetrahedral elements with zero volume, we impose that each tetrahedron contributes with only one face on the approximation $\mathcal{S}_\mathcal{M}$. Thus, we refine all tetrahedra with two or more faces on $\mathcal{S}_\mathcal{M}$, see Figure 6c. Note that the resulting elements have only one face on $\mathcal{S}_\mathcal{M}$, since we have imposed that the faces in $\mathcal{S}_\mathcal{M}$ are parallel to the coordinate planes in the computational space, and we are using the Kossaczký refinement.

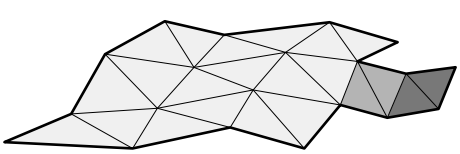

(a) Case 1: marked triangles of $\mathcal{S}_\mathcal{M}$ to be recursively deleted

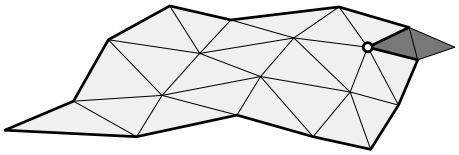

(b) Case 2: marked triangles to be added.

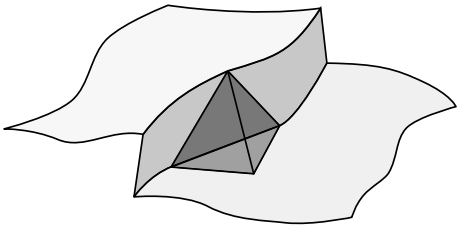

(c) Case 3: tetrahedron to be refined.

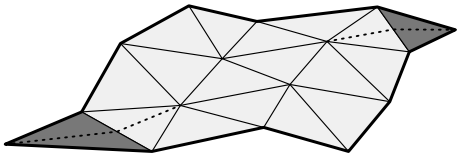

(d) Case 4: marked triangles of $\mathcal{S}_\mathcal{M}$ are refined

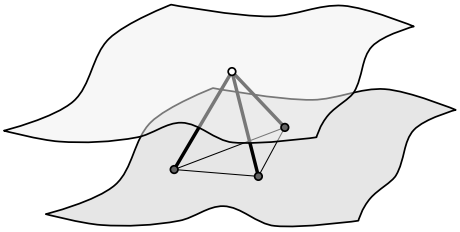

(e) Case 5: marked edges are refined.

Figure 6: Illustration of the five different cases of the surface healing process.

4. *Refine faces of $\mathcal{M}$ with more than one edge at the boundary of $\mathcal{S}_\mathcal{M}$.* In order to avoid faces with a null area at the boundary of $\mathcal{S}_\mathcal{M}$, we impose that each face contributes to the boundary of $\mathcal{S}_\mathcal{M}$ with only one edge. To solve this issue, we refine such faces, see Figure 6d.

5. *Refine edges with nodes on different surfaces.* When the nodes of an edge belong to different surfaces (immersed or boundary surface), it may be difficult to optimize the quality of the mesh and obtain high-quality elements. Hence, we refine such edges of the mesh to give more freedom to the optimization process, see Figure 6e.

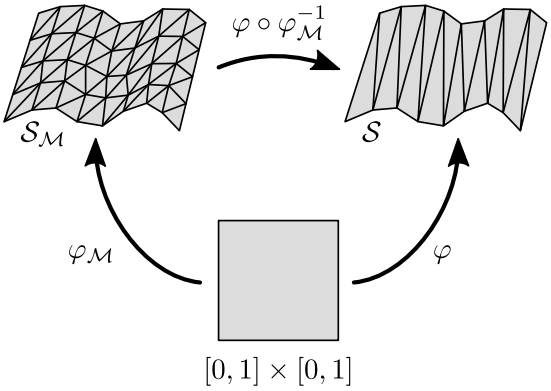

Figure 7: Surface projection diagram.

3.6. Surface Projection

The next step consists on projecting the nodes of $\mathcal{S}_{\mathcal{M}}$ onto $\mathcal{S}$. At the end of this step, all of the nodes in $\mathcal{S}_{\mathcal{M}}$ will be located on the target surface $\mathcal{S}$.

First, we compute the Floater parameterizations [17] of $\mathcal{S}$ and $\mathcal{S}_{\mathcal{M}}$, denoted by $\boldsymbol{\varphi}$ and $\boldsymbol{\varphi}_{\mathcal{M}}$, respectively, as

$$\boldsymbol{\varphi} : \mathcal{U} \to \mathcal{S}, \qquad \boldsymbol{\varphi}_{\mathcal{M}} : \mathcal{U} \to \mathcal{S}_{\mathcal{M}}, \tag{3}$$

where $\mathcal{U} = [0,1] \times [0,1]$ is a common parametric space for both surfaces, see Figure 7. Then, each node of $\mathcal{S}_{\mathcal{M}}$, $\mathbf{x}_i$, is moved to the new position, $\mathbf{x}'_i$ according to:

$$\mathbf{x}'_i = \boldsymbol{\varphi} \circ \boldsymbol{\varphi}_{\mathcal{M}}^{-1}(\mathbf{x}_i) \tag{4}$$

Note that this projection procedure has several advantages. We avoid to solve a non-linear projection problem for each node to projected. Instead, we solve two linear problems to compute the mappings of $\mathcal{S}_{\mathcal{M}}$ and $\mathcal{S}$. Moreover, we obtain the parametric coordinates of the projected nodes on $\mathcal{S}$. This information is necessary to perform the untangling and smoothing process, detailed in the next section.

3.7. Mesh Optimization

After the projection process, inverted and low-quality elements may appear. Thus, to obtain a valid and high-quality mesh, we apply an optimization procedure based on the untangling and smoothing technique proposed in [18]. Moreover, we add the capability to optimize the mesh quality by moving the location

of inner, edge and surface nodes, according to [19]. Note that the result of the optimization problem defines a high-quality volumetric mapping between the computational domain and the physical domain in which the inserted surfaces are interpolated.

3.7.1. Regularized Shape Distortion Measure

According to [22], the shape distortion measure is defined as

$$\eta_E(\boldsymbol{J\phi}) = \frac{\|\boldsymbol{J\phi}\|^2}{3|\sigma(\boldsymbol{J\phi})|^{\frac{2}{3}}} \tag{5}$$

where $\boldsymbol{\phi}$ is the affine mapping between the ideal element E^I and the physical element, E^P, $\boldsymbol{J\phi}$ is the Jacobian matrix of $\boldsymbol{\phi}$, $\|\cdot\|$ is the Frobenius norm, and σ is the determinant. In the meccano method, the ideal element of a physical tetrahedron E_i^P is the rectangular tetrahedron that is its counterpart in the computational space E_i^I

$$E_i^I = \mathbf{\Pi}^{-1}(E_i^P) \tag{6}$$

This distortion measure is invariant to translation, rotation, and scale [22]. It takes values in the range $[1, \infty)$, being $\eta = 1$ when the physical and ideal element only differ in the invariants, and $\eta = \infty$ when the physical element is degenerate. The quality of an element is defined as the inverse of the distortion

$$q = \frac{1}{\eta}. \tag{7}$$

Thus, it takes values between 0 (degenerated element) and 1 (ideal element).

The shape distortion measure presents asymptotes when $\sigma(\boldsymbol{J\phi})$, and this prevents its use in a continuous minimization process when inverted elements are present. To overcome this drawback, we use the regularized distortion measure introduced in [23, 18] for linear elements, in which σ is replaced by

$$h(\sigma) = \frac{1}{2}\left(\sigma + \sqrt{\sigma^2 + 4\delta^2}\right) \tag{8}$$

where δ is a small parameter that depends on the problem. This regularization is also used for optimizing curved high-order meshes [24, 25, 19].

3.7.2. Objective Function

The simultaneous untangling and smoothing algorithm is based on the optimization of an objective function defined in terms of the regularized distortion

measure of the elements adjacent to a node. Let $\mathbf{x}$ be the location of the node, and m the number of adjacent tetrahedra. Then, we define the objective function as

$$f(\mathbf{x}) = \sum_{j=1}^{m} \eta_{E_j}(\boldsymbol{J\phi}) \tag{9}$$

where E_j is the j^{th} element adjacent to the node. The derivatives of the objective function are evaluated analytically according to [26].

3.7.3. Objective Function for Surface and Edge Nodes

We need to ensure that edge and surface nodes in the optimized mesh are located on the corresponding entities they belong to. Therefore, we define a new objective function that evaluates the regularized distortion measure of the adjacent tetrahedra in terms of the parametric coordinates of the node, see [19].

For surface nodes, the corresponding objective function becomes

$$f_{\boldsymbol{\varphi}}(\mathbf{u}) = f \circ \boldsymbol{\varphi}(\mathbf{u}), \tag{10}$$

where $\boldsymbol{\varphi}$ and $\mathbf{u}$ are the parameterization and the parametric coordinates of surface $\mathcal{S}$.

Each edge of the model is parameterized using the arc-length parameter, $\boldsymbol{\gamma}(s)$. Thus the objective function for edge nodes is expressed using the parameterization $\boldsymbol{\gamma}(s)$ as

$$f_{\boldsymbol{\gamma}}(s) = f \circ \boldsymbol{\gamma}(s), \tag{11}$$

Note that, the derivatives involved in the optimization process for surface and edge nodes are computed numerically due to the linear piece-wise definition of $\boldsymbol{\varphi}$ and $\boldsymbol{\gamma}$.

We highlight that in the proposed approach, we do not use a distortion measure for the surface triangles, instead we only take into account the quality of the tetrahedral elements. That is, we are computing a valid and high-quality volumetric mapping between the computational domain and the physical domain, such that the surface and edge nodes are constrained to move along the corresponding entities.

3.7.4. Optimization Approach

The optimization approach is devised as a Gauss-Seidel iterative process moving one node at a time. That is, for each node we modify its position while

Algorithm 2 Procedure to smooth a mesh, $\mathcal{M}$.

```
1: function smoothMesh(Mesh M, Real ε)
2:     Boolean isConverged ← false
3:     while not isConverged do
4:         Real disp ← 0
5:         for each free node, n do
6:             Function g ← getObjectiveFuncion(n)    ▷ get edge, surface or
                                                      ▷ inner objective function
7:             Real nodeDisp ← smoothNode(n,g)
8:             disp ← max{disp, nodeDisp}
9:         end for
10:        isConverged ← (disp ≤ maxDisp)
11:    end while
12: end function
```

keeping fixed the position of all the other nodes. The new position is computed by optimizing the corresponding objective function of the node. This optimization is performed using a line-search method in which the search direction is computed using Newton's method, and the step length is computed using the strong Wolfe conditions, see details in [27]. Algorithm 2 details the proposed untangling and smoothing process.

4. Examples

In this section the presented method is applied to three different geometries. The first geometry is an academic example where a curved surface is inserted in a cube. The two last examples are taken from realistic cases where the insertion of the surface in the mesh is needed. In all the examples, we colour the elements according their shape quality, see Equation (5). In addition, for all of them, we present a table that summarizes the shape quality statistics of the mesh elements. Specifically, we provide the number of tangled elements, and the minimum, maximum, mean and standard deviation of the element quality. We highlight that in all cases the cases the final mesh is a valid high-quality mesh, where the insertion of the surfaces has not drastically decreased the quality of

the initial mesh.

4.1. Simple Cube

The first example deals with the insertion of a sinusoidal surface inside a tetrahedral mesh for a cube, $\mathcal{M}$, see Figure 8a. Figure 8b shows the refined tetrahedral mesh and the initial approximating surface, $\mathcal{S}_{\mathcal{M}}$, extracted from triangles of $\mathcal{M}$. Note that at this stage, the candidate triangles to approximate the surface are parallel to the coordinate planes of the computational domain. Then, the nodes of $\mathcal{S}_{\mathcal{M}}$ are projected onto the immersed surface, $\mathcal{S}$, see Figure 8c. Low-quality and inverted elements appear near the projected surface, due to the movement of the nodes. Finally, the whole mesh is optimized using the presented optimization method in order to repair the tangled elements and improve the overall mesh quality, see Figure 8d. It is important to remark that the smoother moves all the interior nodes of the mesh, including the ones that are located on $\mathcal{S}_{\mathcal{M}}$. In this case, such nodes are able to slide along the surface $\mathcal{S}$. This is a key point in order to obtain a valid and high-quality tetrahedral mesh, specially around the high-curvature areas of the inserted surface, where the feasible region is small.

Figures 9a, 9b, and 9c, present the distribution of the elements according to their shape quality for the mesh before inserting the surface (Figure 8a), the mesh once the nodes are projected onto the surface (Figure 8c), and the mesh after applying the proposed smoother (Figure 8d). In this example, all the elements before inserting the surface have a quality of 1.0. The projection of nodes introduces low-quality and inverted elements. Then, the smoothing process increases the overall mesh quality. Table 1 details the mesh quality statistics. As it has been pointed out, all the elements of the initial mesh are of the highest quality. The projection process has introduced 58 inverted elements and therefore, the minimum quality is 0. Although the maximum quality is 1, this mesh is not valid for any simulation process. Once the mesh is optimized, there are not any inverted elements, and the minimum and mean quality are increased to 0.35 and 0.92, respectively. The maximum quality is decreased to 0.99 in order to accommodate the displacement of the nodes during the optimization process. Also, the standard deviation is decreased by a factor of 3. The final mesh contains elements with lower quality than the initial mesh.

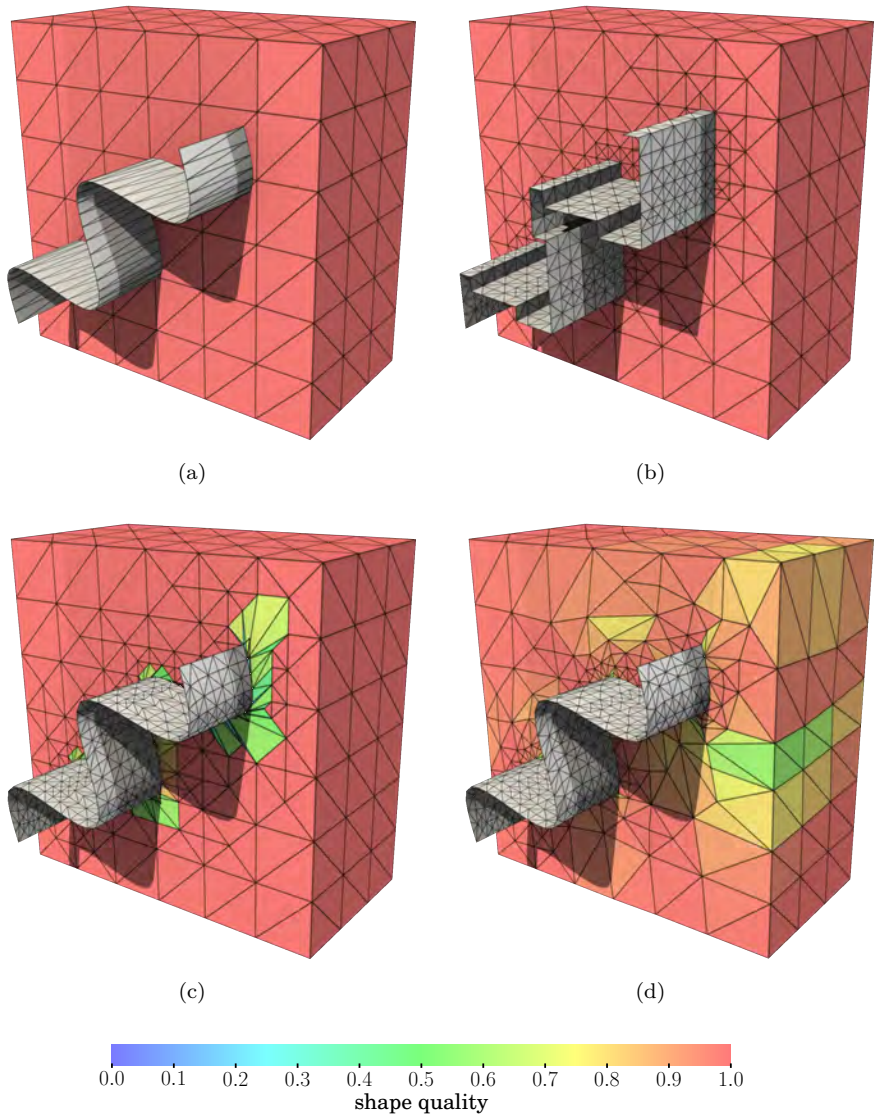

Figure 8: Approximation of an immersed sinusoidal surface, $\mathcal{S}$, in a tetrahedral mesh for a cube: (a) initial tetrahedral mesh and surface to be inserted; (b) refined tetrahedral mesh and initial $\mathcal{S}_\mathcal{M}$ extracted from triangles of $\mathcal{M}$; (c) nodes form $\mathcal{S}_\mathcal{M}$ projected onto $\mathcal{S}$; and (d) smoothed final mesh.

In this example, this is expected since the initial mesh is entirely composed of ideal elements.

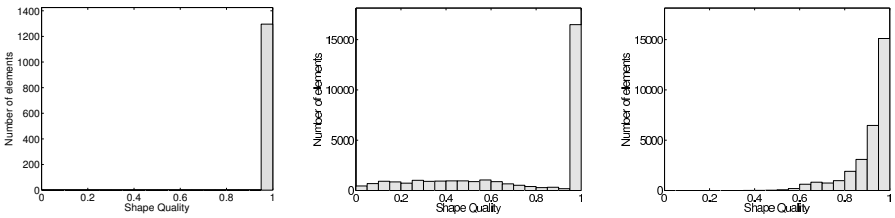

(a) (b) (c)

Figure 9: Mesh quality histogram for: (a) initial mesh; (b) mesh with immersed surfaces before optimization; and (c) mesh with immersed surfaces after optimization;

4.2. Faults Insertion

The second example deals with the insertion of fault surfaces into a discretized sub-soil model, see Figure 10. The tetrahedra of the mesh are not able to resolve the geometric features of the inserted surface. This example shows that the proposed method does not depend on the element size of the initial mesh. Figure 11 shows the different stages of the insertion surface algorithm for the last inserted fault (red surface in Figure 10). First, we refine the mesh and select the candidate triangles to approximate the surface, Figure 11a. Then, we apply the proposed projection algorithm to map the selected nodes onto the inserted surface, Figure 11b. This step generates inverted and low-quality elements. Thus, we apply the presented untangling and smoothing algorithm to repair the inverted elements and increase the overall mesh quality, see Figure 11c.

Figures 12a, 12b, and 12c show the quality histogram of the mesh before inserting the surface, the mesh once the nodes are projected onto the surface (Figure 11b), and the mesh after applying the proposed smoother (Figure 11c). The histogram is similar for both meshes where the number of elements increase with the quality, being the more frequent qualities the highest interval. The main differences is the dispersion of the qualities. The qualities in the initial mesh are more concentrated towards the highest values whilst the qualities in the final mesh are more dispersed. Figure 12b shows the quality decay due to the projection process where some elements are not valid. Nevertheless, the applied smoother increases the overall mesh quality. These remarks can be observed quantitatively in Table 1. Comparing the initial and final mesh

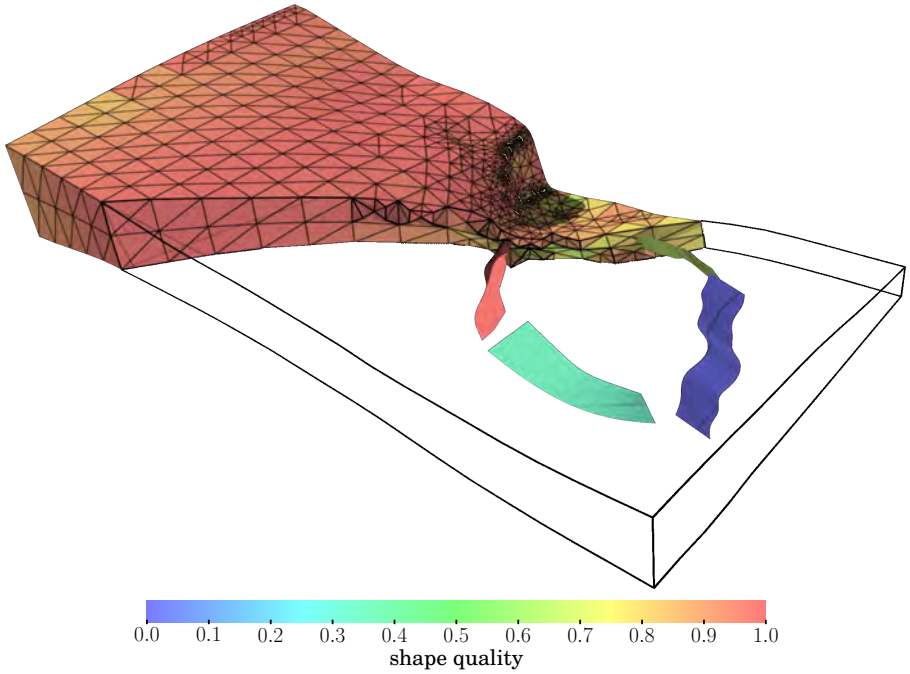

Figure 10: Initial tetrahedral mesh for a sub-soil model, elements coloured according their quality, and the four faults to be inserted.

quality statistics, both the minimum and mean qualities have decreased—from 0.26 to 0.13, and from 0.92 to 0.81 respectively—and the standard deviation has increased—from 0.09 to 0.14.These results agree with the qualitative observations. The optimization improvement is clear from comparing the projected and final statistics; the minimum and mean quality have increased from 0 to 0.13, and from 0.77 to 0.81, respectively, and the standard deviation has decreased from 0.21 to 0.14.

4.3. Atmospheric Layer Insertion

In several atmospheric applications it is usual to create a base mesh and then adapt it to each specific simulation. In this example, we will use a given tetrahedral mesh of the East zone of the Gran Canaria island (Spain) to simulate the transport and reaction of pollutants in the atmosphere. In particular, we are interested in the distribution of pollutant concentration on two surfaces that are an extrusion of the orography of the terrain. Therefore, we will use the proposed method to insert them and we will show that the resulting mesh

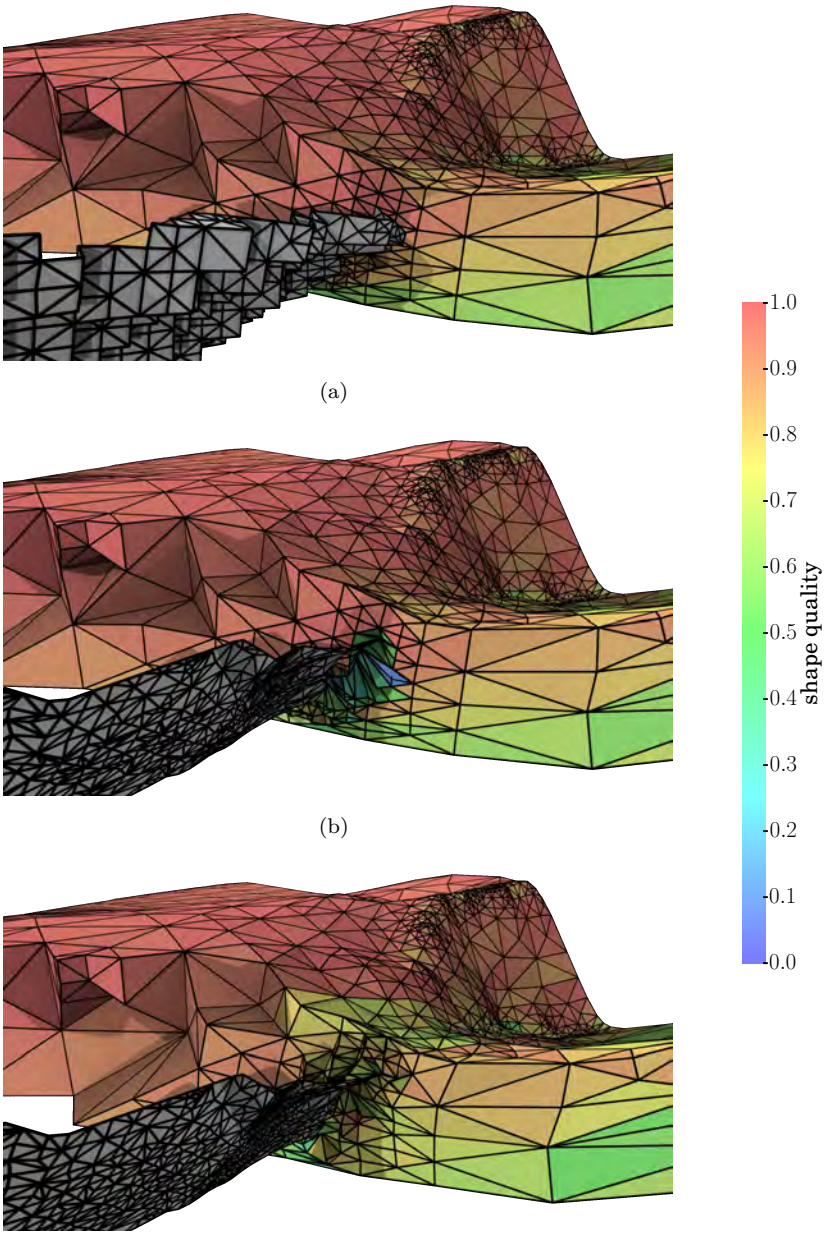

Figure 11: Approximation of the fourth immersed fault, $\mathcal{S}$, in a tetrahedral mesh for a sub-soil model: (a) refined tetrahedral mesh and initial $\mathcal{S}_{\mathcal{M}}$ extracted from triangles of $\mathcal{M}$; (b) nodes form $\mathcal{S}_{\mathcal{M}}$ projected onto $\mathcal{S}$; and (c) smoothed final mesh.

is valid for simulation purposes.

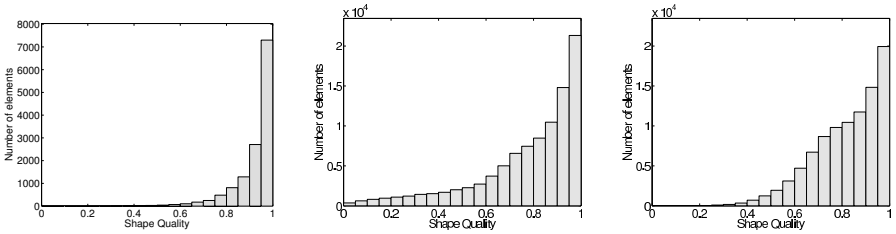

(a) (b) (c)

Figure 12: Mesh quality histogram for: (a) initial mesh; (b) mesh with immersed surfaces before optimization; and (c) mesh with immersed surfaces after optimization;

4.3.1. Mesh generation

Figure 13 shows the orography of the considered area in the East part of Gran Canaria island and the immersed surfaces. They are located at 1000 and 2000 meters above the terrain. Similar to the previous examples, Figure 14 illustrates the different stages of the insertion surface algorithm. In this figure, the inserted surface is the highest one (red in Figure 13). Figure 14a shows the refinement and selection step, Figure 14b presents the projection of the selected mesh onto the inserted surface where low-quality and tangled elements appear; and finally the resulting mesh, after the untangling and smoothing algorithm, see Figure 14c.

Figure 15 shows the quality histogram of the mesh before inserting the second surface, once the nodes are projected onto the second surface (Figure 14b), and after applying the proposed smoother (Figure 14c). In this case, comparing the initial and final meshes, the dispersion of the qualities has increased and the minimum quality has decreased. This observation agrees with the Faults insertion example, although in this case the differences are smaller. Regarding the projected and final meshes, we highlight that the optimization process has repaired all the tangled elements, and the minimum quality has improved. The main statistical values of the mesh quality are detailed in Table 1. Comparing the initial (before inserting any surface) and final meshes, we observe that the minimum quality has decreased from 0.58 to 0.32, that the maximum and mean qualities have detracted slightly from 1 to 0.99 and from 0.97 to 0.95 respectively, and that the standard deviation has increased from 0.03 to 0.08. As in the

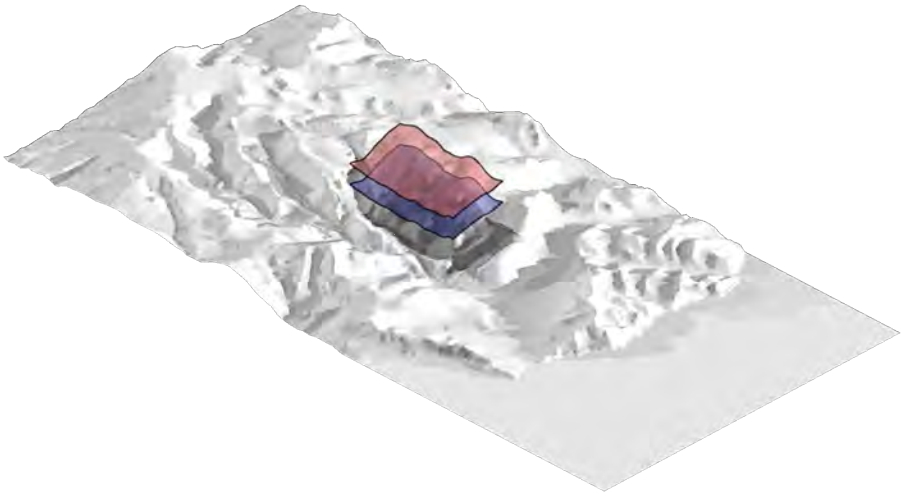

Figure 13: East zone of Gran Canaria island and the two surfaces to be inserted.

previous examples, the optimization process has improved the quality repairing 6585 non-valid elements, increasing the minimum and mean quality from 0 to 0.32 and from 0.89 to 0.95 respectively; and decreasing the standard deviation from 0.21 to 0.08.

4.3.2. Transport and reaction of pollutants

Once the mesh with the surfaces is generated we simulate the transport and reaction of pollutants. In this case, we assume that a pollutant leak from a ship in the sea is transported into the island by a wind field. We know that the general direction of the wind field is from East to West (from sea to the island). To generate a more realistic wind field we use a mass-consistent wind model [28, 29] that assumes constant density and verifies the continuity equation (mass conservation) in the domain and impermeability on the terrain.

Using the resulting wind field, we simulate the transport and reaction of pollutants. A finite element model designed to simulate the microscale [30, 31] is used in this example. This model uses a finite element method stabilized with least squares [32] to prevent the numerical oscillations that arise with the classical Galerkin formulation. The resulting linear system has a symmetric matrix and we solve it using the conjugate gradient method preconditioned

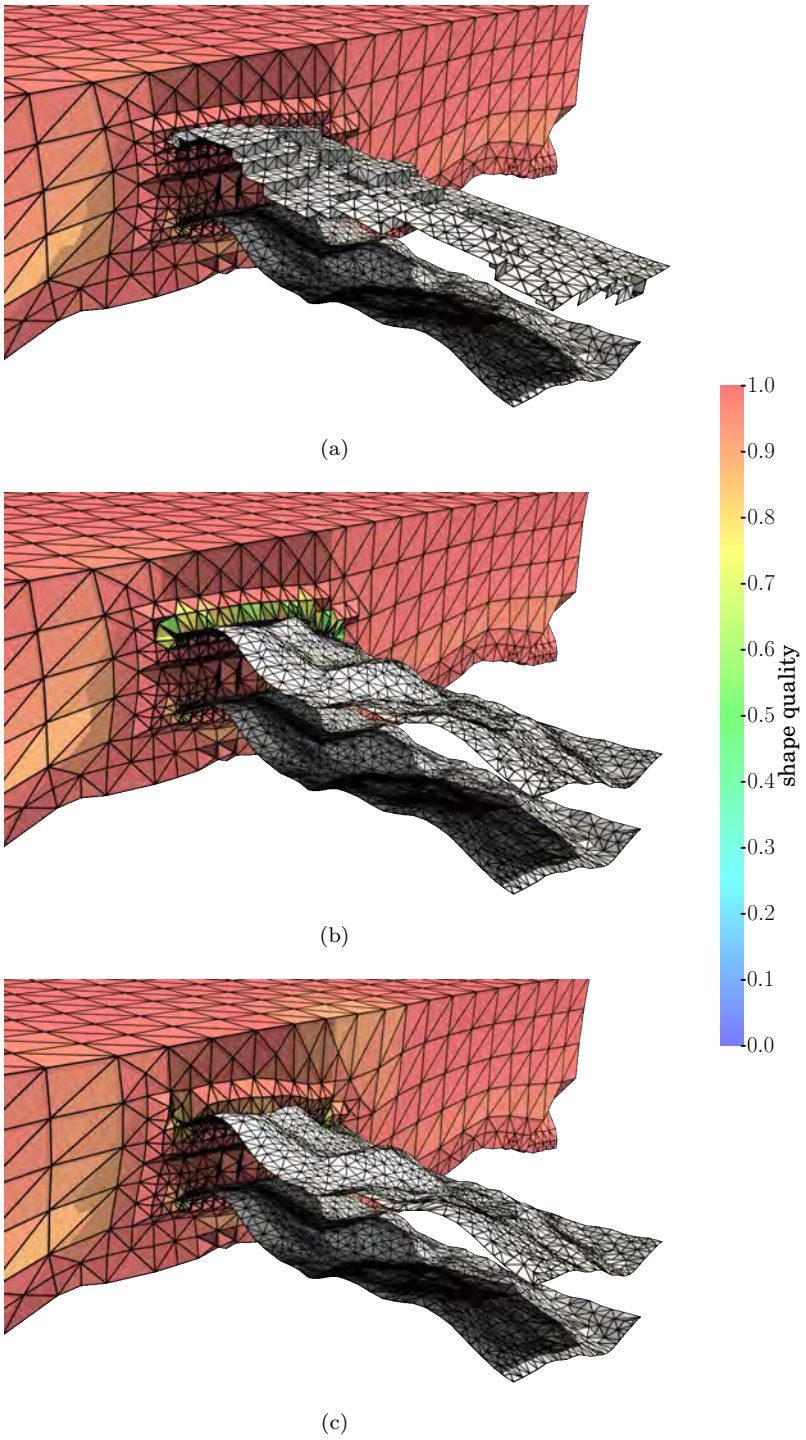

Figure 14: Approximation of the second immersed surface, $\mathcal{S}$, in a tetrahedral mesh for an air quality model: (a) refined tetrahedral mesh and initial $\mathcal{S}_{\mathcal{M}}$ extracted from triangles of $\mathcal{M}$; (b) nodes form $\mathcal{S}_{\mathcal{M}}$ projected onto $\mathcal{S}$; and (c) smoothed final mesh.

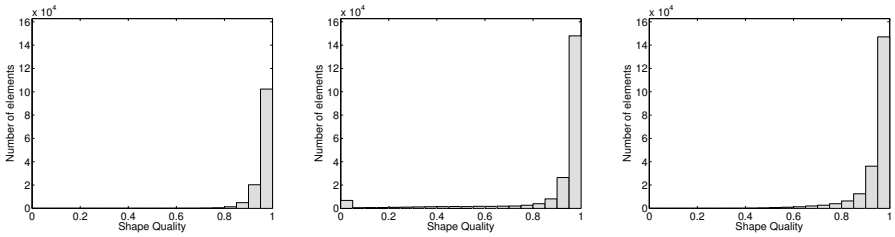

(a) (b) (c)

Figure 15: Mesh quality histogram for: (a) initial mesh; (b) mesh with immersed surfaces before optimization; and (c) mesh with immersed surfaces after optimization;

with an incomplete Cholesky factorization density type [33, 34].

The prescribed boundary conditions for the pollutant concentration are the following: a Dirichlet condition of $0.5\,\mathrm{g\,m^{-3}}$ at a region of the sea boundary, a null Dirichlet condition in the inflow boundary—we assume that the air outside the area of interest is clean, a natural Neumann condition on the outflow boundaries, and a dry deposition velocity of $0.5\,\mathrm{m\,s^{-1}}$ in the terrain. We use typical diffusion values with a horizontal diffusion of $10\,\mathrm{m^2\,s^{-1}}$ and a vertical of $5\,\mathrm{m^2\,s^{-1}}$.

Figure 16 shows the resulting wind field and the isosurfaces of pollutant concentration after 5 min, 30 min and 60 min. Note that the impermeability condition in the terrain channels the wind field into the valleys and circle the mountains. Looking at the pollutant concentrations, we observe that the front of the plume is transported along the domain and the smaller concentrations flow up to the valleys when the pollutant plume evolves. To highlight the properties of the surface insertion algorithm, we have not applied an automatic mesh refinement to capture the plume front as suggested in [35].

The output of interest is the distribution of the pollutant on the inserted surfaces. Figure 17a shows the concentration after 30 minutes—it corresponds to Figure 16b. At this moment, the front of the $0.5\,\mathrm{g\,m^{-3}}$ concentration is crossing the bottom surface. Note that the pollutant concentration is smaller on the top layer. Figure 17b shows the distribution after one hour when the plume has developed completely—it corresponds to Figure 16c. At this stage, we observe that the distribution on both surfaces is similar, although the concentration

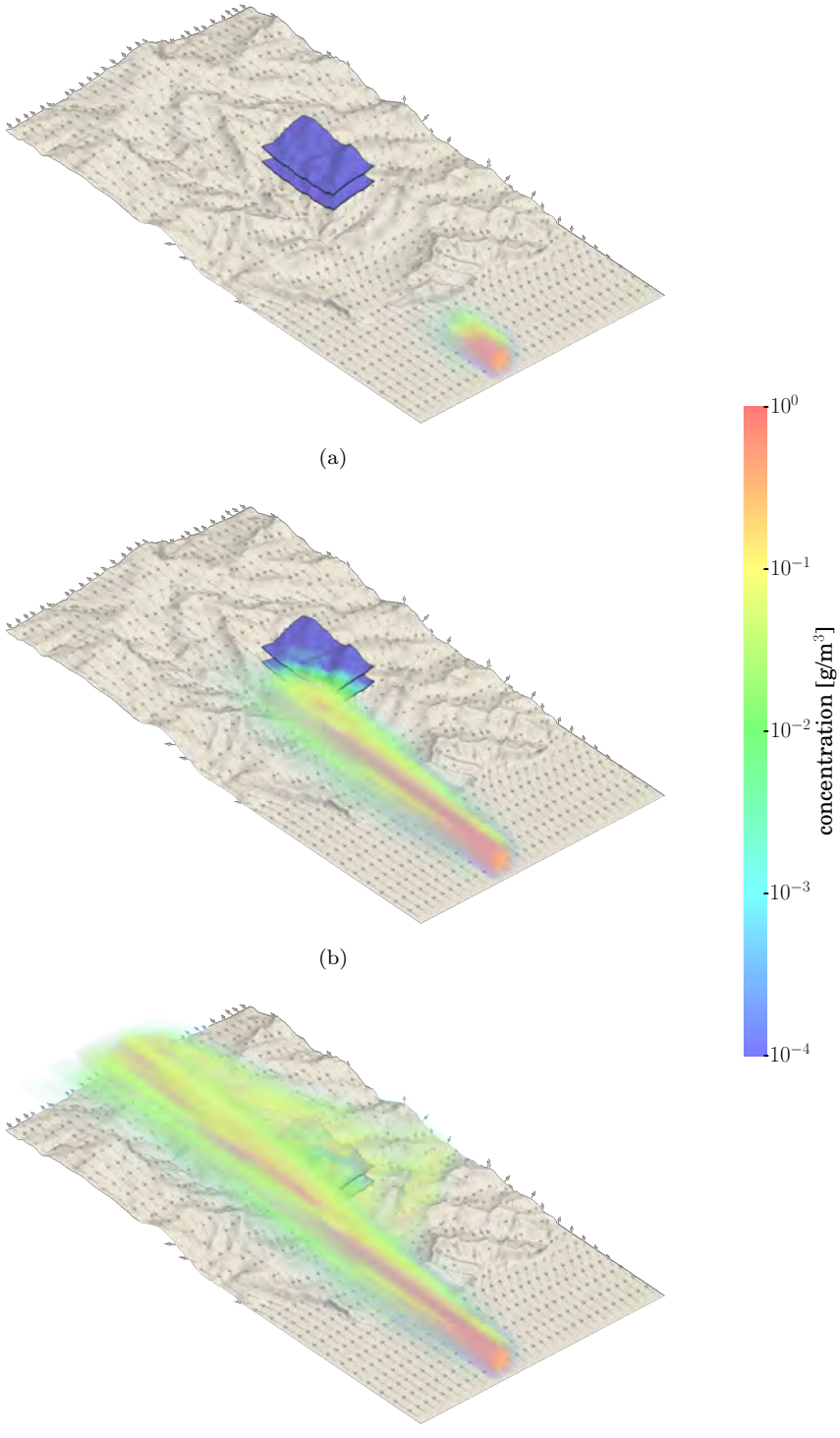

(a)

(b)

(c)

Figure 16: Slice of the isosurfaces of pollutant concentration after (a) five minutes; (b) thirty minutes; (c) one hour.

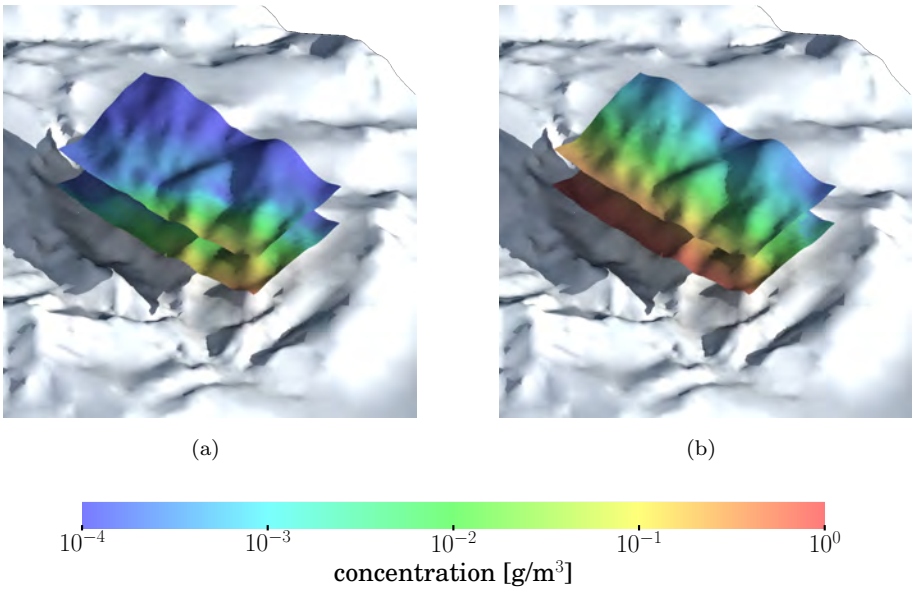

Figure 17: Pollutant concentration distribution in the inserted surfaces after (a) thirty minutes and (b) one hour.

Table 1: Element quality statistics of the presented high-order meshes.

	sinusoidal			sub-soil fault			atmospheric layer		
	original	projected	smoothed	original	projected	smoothed	original	projected	smoothed
inverted	0	58	0	0	1	0	0	6585	0
min	1	0	0.35	0.26	0	0.13	0.58	0	0.32
max	1	1	0.99	0.99	0.99	0.99	1.00	0.99	0.99
mean	1	0.74	0.92	0.92	0.77	0.81	0.97	0.89	0.95
std dev	0	0.33	0.10	0.09	0.21	0.14	0.03	0.22	0.08

values are smaller on the top surface due to the distance to the centre of the plume and wind direction.

This example has shown the applicability of the proposed surface insertion method where the quantity of interest is on the immersed surface.

5. Conclusions

In this work, we propose a novel approach to insert several triangulated surfaces into an existing tetrahedral meccano mesh. The inserted surfaces are approximated using triangles extracted from the tetrahedral mesh. To properly approximate the geometric features of each inserted surface, we propose to apply

a refinement process to the tetrahedral mesh. Thus, we avoid the dependence of the proposed algorithm on the element size of the initial tetrahedral mesh. Then, we select the candidate triangles and project them onto each surface using a novel projection algorithm based on the Floater parameterization. The key idea is to parameterize the initial surface and the approximating surface with the same parametric space. Finally, an untangling and smoothing technique is applied to repair the tangled elements and improve the overall mesh quality. We move the nodes on the edges and surfaces (inner and boundary surfaces) taking into account only the quality of the tetrahedral elements. To this end, we express the objective function in terms of the parametric coordinates of the moving edge surface nodes. We have shown that the proposed method generates high-quality meshes that can be used in numerical simulations.

The presented algorithm has been developed for inserting triangulated surfaces. Nevertheless, the same presented algorithm can deal with parameterized surfaces coming from a CAD model. The only restriction is that the CAD surface has to be simply-connected (no holes) and non-trimmed, in order to define a quadrilateral parametric domain.

Several aspects of the presented method can be improved in order to deal with more complex situations. First, the proposed algorithm does not deal with the insertion of intersecting surfaces, because we do not prescribe the approximation of the intersection between these surfaces. Moreover, since we are using a square parametric domain to perform the projection and smoothing process, we require that the surfaces to be inserted have to be simply-connected surfaces with boundary. Nevertheless, one possible solution is to divide the initial surfaces into simply-connected patches with boundary.

Acknowledgements

This work has been supported by FEDER and the Spanish Government, "Ministerio de Economía y Competitividad" grant contracts: CTM2014-55014-C3-1-R, CTM2014-55014-C3-3-R, CGL2011-29396-C03-01, CGL2008-06003-03-01, CGL2008-06003-03-02, UNLP08-3E-010, CSD2006-00032C; and by CONACYT-SENER ("Fondo Sectorial CONACYT SENER HIDROCARBUROS", grant contract: 163723).

References

[1] Ohno M, Matsuura K. Quantitative phase-field modeling for dilute alloy solidification involving diffusion in the solid. Physical Review E 2009;79(3):031603.

[2] Hachem E, Feghali S, Coupez T, Codina R. A three-field stabilized finite element method for fluid-structure interaction: elastic solid and rigid body limit. International Journal for Numerical Methods in Engineering 2015;104(7):566–84.

[3] Amiri F, Millán D, Arroyo M, Silani M, Rabczuk T. Fourth order phase-field model for local max-ent approximants applied to crack propagation. Computer Methods in Applied Mechanics and Engineering 2016;.

[4] Moës N, Dolbow J, Belytschko T. A finite element method for crack growth without remeshing. International journal for numerical methods in engineering 1999;46(1):131–50.

[5] Zlotnik S, Díez P. Hierarchical x-fem for n-phase flow (n> 2). Computer Methods in Applied Mechanics and Engineering 2009;198(30):2329–38.

[6] Tamayo-Mas E, Rodríguez-Ferran A. A medial-axis-based model for propagating cracks in a regularised bulk. International Journal for Numerical Methods in Engineering 2015;101(7):489–520. URL: http://dx.doi.org/10.1002/nme.4757. doi:10.1002/nme.4757.

[7] Rangarajan R, Lew A. Universal meshes: A new paradigm for computing with nonconforming triangulations. 2012. arXiv:1201.4903.

[8] Rangarajan R, Lew AJ. Universal meshes: A method for triangulating planar curved domains immersed in nonconforming meshes. International Journal for Numerical Methods in Engineering 2014;98(4):236–64. doi:10.1002/nme.4624.

[9] Rangarajan R, Chiaramonte MM, Hunsweck MJ, Shen Y, Lew AJ. Simulating curvilinear crack propagation in two dimensions with universal meshes. International Journal for Numerical Methods in Engineering 2015;102(3-4):632–70.

[10] Zaide DW, Ollivier-Gooch CF. Inserting a curve into an existing two dimensional unstructured mesh. In: Proceedings of the 22nd International Meshing Roundtable. 2014, p. 93–107. doi:10.1007/978-3-319-02335-9_6.

[11] Zaide DW, Ollivier-Gooch CF. Inserting a surface into an existing unstructured mesh. International Journal for Numerical Methods in Engineering 2015;.

[12] Bonfiglioli A, Grottadaurea M, Paciorri R, Sabetta F. An unstructured, three-dimensional, shock-fitting solver for hypersonic flows. Computers & Fluids 2013;73:162–74.

[13] Montenegro R, Cascón JM, Escobar JM, Rodríguez E, Montero G. An automatic strategy for adaptive tetrahedral mesh generation. Applied Numerical Mathematics 2009;59(9):2203–17. doi:10.1016/j.apnum.2008.12.010.

[14] Montenegro R, Cascón JM, Escobar JM, Rodríguez E, Montero G. The meccano method for simultaneous volume parametrization and mesh generation of complex solids. IOP Conference Series: Materials Science and Engineering 2010;10(1):012–8. doi:10.1088/1757-899X/10/1/012018.

[15] Montenegro R, Cascón JM, Rodríguez E, Escobar JM, Montero G. The meccano method for automatic three-dimensional triangulation and volume parametrization of complex solids. In: Topping B, Adam J, Pallarés F, Bru R, Romero M, editors. Developments and Applications in Engineering Computational Technology; chap. 2; seventh ed. Stirlingshire: Saxe-Coburg Publications. ISBN 978-1-874672-48-7; 2010, p. 19–48. doi:10.4203/csets.26.2.

[16] Cascón JM, Rodríguez E, Escobar JM, Montenegro R. Comparison of the meccano method with standard mesh generation techniques. Engineering with Computers 2015;31(1):161–74. doi:10.1007/s00366-013-0338-6.

[17] Floater MS. Mean value coordinates. Computer Aided Geometric Design 2003;20(1):19–27. doi:10.1016/S0167-8396(03)00002-5.

[18] Escobar JM, Rodríguez E, Montenegro R, Montero G, González-Yuste JM. Simultaneous untangling and smoothing of tetrahedral meshes. Com-

puter Methods in Applied Mechanics and Engineering 2003;192(25):2775–87. doi:10.1016/S0045-7825(03)00299-8.

[19] Ruiz-Gironés E, Roca X, Sarrate J. High-order mesh curving by distortion minimization with boundary nodes free to slide on a 3D CAD representation. Computer-Aided Design 2016;72:52–64. doi:10.1016/j.cad.2015.06.011.

[20] Kossaczký I. A recursive approach to local mesh refinement in two and three dimensions. Journal of Computational and Applied Mathematics 1994;55(3):275–88. doi:10.1016/0377-0427(94)90034-5.

[21] Escobar JM, Rodríguez E, Montenegro R, Montero G, González-Yuste JM. SUS code: simultaneous mesh untangling and smoothing code. http://www.dca.iusiani.ulpgc.es/SUScode; 2010.

[22] Knupp PM. Algebraic mesh quality metrics. SIAM J Sci Comput 2001;23(1):193–218. doi:10.1137/s1064827500371499.

[23] Garanzha V, Kaporin I. Regularization of the barrier variational method. Computational mathematics and mathematical physics 1999;39(9):1426–40.

[24] Gargallo-Peiró A, Roca X, Peraire J, Sarrate J. Optimization of a regularized distortion measure to generate curved high-order unstructured tetrahedral meshes. International Journal for Numerical Methods in Engineering 2015;103(5):342–63. URL: http://dx.doi.org/10.1002/nme.4888. doi:10.1002/nme.4888.

[25] Gargallo-Peiró A, Roca X, Peraire J, Sarrate J. A distortion measure to validate and generate curved high-order meshes on cad surfaces with independence of parameterization. International Journal for Numerical Methods in Engineering 2015;.

[26] Ruiz-Gironés E, Roca X, Sarrate J, Montenegro R, Escobar JM. Simultaneous untangling and smoothing of quadrilateral and hexahedral meshes using an object-oriented framework. Advances in Engineering Software 2015;80:12–24.

[27] Dennis JE, Schnabel RB. Numerical Methods for Unconstrained Optimization and Nonlinear Equations. Society for Industrial & Applied Mathematics (SIAM); 1996. doi:10.1137/1.9781611971200.

[28] Ferragut L, Montenegro R, Montero G, Rodríguez E, Asensio M, Escobar JM. Comparison between 2.5-D and 3-D realistic models for wind field adjustment. Journal of Wind Engineering and Industrial Aerodynamics 2010;98(10-11):548–58. doi:10.1016/j.jweia.2010.04.004.

[29] Oliver A, Rodríguez E, Escobar JM, Montero G, Hortal M, Calvo J, et al. Wind forecasting based on the HARMONIE model and adaptive finite elements. Pure and Applied Geophysics 2015;172(1):109–20. doi:10.1007/s00024-014-0913-9.

[30] Oliver A, Montero G, Montenegro R, Rodríguez E, Escobar JM, Pérez-Foguet A. Finite element simulation of a local scale air quality model over complex terrain. Advances in Science and Research 2012;8:105–13. doi:10.5194/asr-8-105-2012.

[31] Oliver A, Montero G, Montenegro R, Rodríguez E, Escobar JM, Pérez-Foguet A. Adaptive finite element simulation of stack pollutant emissions over complex terrains. Energy 2013;49(0):47–60. doi:10.1016/j.energy.2012.10.051.

[32] Jiang B. The Least-Squares Finite Element Method. Springer Berlin Heidelberg; 1998. doi:10.1007/978-3-662-03740-9.

[33] Lin CJ, Moré JJ. Incomplete Cholesky factorizations with limited memory. SIAM Journal on Scientific Computing 1999;21(1):24–45. doi:10.1137/S1064827597327334.

[34] Rodríguez-Ferran A, Sandoval M. Numerical performance of incomplete factorizations for 3D transient convection–diffusion problems. Advances in Engineering Software 2007;38(6):439–50. doi:10.1016/j.advengsoft.2006.09.003.

[35] Monforte L, Pérez-Foguet A. Esquema adaptativo para problemas tridimensionales de convección-difusión. Revista Internacional de Métodos

Numéricos para Cálculo y Diseño en Ingeniería 2014;30(1):60–7. doi:10.1016/j.rimni.2012.11.003.